

## Collective soliton collision annihilation and related collisional statistics in a figure-8 Tm-doped fiber laser

Jin Jer Huang<sup>1,\*</sup>, Min Yang,<sup>1</sup> Jian Zheng Lin<sup>2</sup>, Bo Yang Su<sup>2</sup>, and Xin Lu Zhang<sup>2,†</sup>

<sup>1</sup>*Department of Applied Physics, Tiangong University, Tianjin 300387, China*

<sup>2</sup>*Department of Optoelectronic Information Science and Engineering, Tiangong University, Tianjin 300387, China*



(Received 15 December 2023; accepted 27 February 2024; published 19 March 2024)

We report an unusual collision-induced collective annihilation of solitons at 2  $\mu\text{m}$  in a figure-8 Tm-doped fiber laser. The solitons are generated in a unique bidirectional soliton rain state, where the interaction of heterogeneous vector solitons stimulates deep inelastic collisions. The experiment shows that the solitons activate four collisional scenarios and eventually are annihilated after an average of three to four collisions, adhering to a geometric distribution. The collision-annihilation state can be maintained even for certain energy perturbations, unveiling an extreme soliton characteristic in a large anomalous-dispersion regime.

DOI: [10.1103/PhysRevA.109.033520](https://doi.org/10.1103/PhysRevA.109.033520)

### I. INTRODUCTION

Solitons, as condensed states of fields or matter, exist widely in physics [1]. Optical solitons in fibers, because of their prevalence in laser systems and communication lines, have been intensively studied in theory and application [2]. Classical temporal solitons, also known as Kerr solitons or simply solitons, exist in only anomalous dispersive waveguides. A spontaneous balance between dispersion and self-phase modulation gives rise to a soliton, which can be described as a particlelike state in the solutions of the nonlinear Schrödinger equation (NSE) and the Ginzburg-Landau equation (GLE) [3]. In the case of a cavity GLE, the soliton carries sidebands or a field known as the dispersive wave (DW), similar to a charged particle's associated field. The solitons exhibit various interactions with other light waves, including unique collision mechanisms with each other [3]. The interactions forms numerous multisoliton states of bound, loosely bound, and unbound bundles, depending on the forces exerted by the solitons and the DWs between them [4–7]. The DW, continuous wave, and background noise can drive the soliton by varying its strength, duration, phase, and group velocity (frequency) through moderate interactions [8–13]. A similar phenomenon also occurs in a dissipative cavity, where nonstationary solitons in lumped cases vary under a disturbance but are able to stabilize themselves by periodically shedding and acquiring DWs, thereby renewing resonant sidebands [8,12,14,15]. Despite the rare occurrence of quenching in a strongly dissipative cavity [16], solitons demonstrate overall robustness, enabling them to withstand various impacts, such as gain, depletion, dispersion management, and even direct collision.

Soliton collisions reflect an essential nonlinear interaction that has many analogs in physics, such as sine-Gordon soli-

tons [17], matter waves in ultracold atoms [18,19], spatial solitons [20,21], and collisions between different types [22]. The focus here is on the collision dynamics of fundamental Kerr solitons from mode-locked fiber lasers, which can be supported simultaneously by coupled NSEs and GLEs. Due to the potential of soliton communication, extensive research has been devoted to soliton collision dynamics. Early on, research on stable orthogonally polarized soliton states revealed that pairwise solitons in birefringent fibers couple through a complex nonlinear interaction with oscillating forces [23], resulting in both elastic and inelastic collisions [24–36]. The postcollision solitons were predicted by theory to change in phase, frequency [32–35], polarization (shadow) [29–31], and amplitude (exchanging energy) [27,32,35,37]. It was also found that solitons in the collision region interact like some resonant modes [32,36,38], depending on their initial phases. Since the introduction of Hirota's bilinearization method by Radhakrishnan and Lakshmanan [39], related theoretical studies on dual- or multisoliton collisions have been initiated. They include research on the Manakov model [35], as well as on higher-order [40–43], four-wave mixed [44], multimode ( $> 2$ ) [45,46], and mode-mixed [47,48] coupled NSEs. Apart from volatile positions, chirps, and amplitude-dependent phase and frequency shifts [49], there is a robust common characteristic of the shape-changing intensity redistributions after an inelastic collision [50] under strong environmental perturbations of fiber loss and modified cross-phase modulation. The good switching property demonstrated possible applications in soliton-based optical logic gates [51]. Approximation [14,23,52] and numerical [53–56] methods also help us to understand soliton dynamics. So far, related simulations have predicted collisionless energy exchange with third-order dispersion [57], soliton fusion [55] and fission [54,58], inelastic singlet-molecule soliton collision [59], and conversation of total polarization [60].

Ten years ago, experimental observations of soliton dynamics were rarely conducted due to the lack of effective ultrafast metrology. However, with the maturity of time-

\*huangjinzhe@tiangong.edu.cn

†zhangxinlu@tiangong.edu.cn

resolved spectral technology (the time-stretched dispersive Fourier-transform method [61,62]), transient intersoliton microdynamics have recently experienced a resurgence in the work of Herink *et al.* [63] and Krupa *et al.* [64]. Kerr soliton molecules demonstrated highly complex excitations, both periodic and aperiodic, inside a bound soliton pair associated with a possible topology protection [63], which inspired further investigations [65–73]. On the one hand, these experiments illustrated robust elastic soliton collisions independent of relative phase [65], even through drastic coupling with the energy exchange [66]. On the other hand, they also indicated deeply dissipative inelastic collisions, such as soliton fusion [67]. Additionally, some inelastic singlet-molecule and intermolecular collisions were observed as well, involving soliton acceleration, abrupt molecule momentum changes, bond exchange by collision, molecule dissociation and recombination [68–71], explosionlike chaotic interaction [72], and reversible transition of Hopf-type bifurcations during the collision of soliton molecules [73].

Even though elastic collisions commonly occur in cavities, in some rare extreme cases, the inelastic dissipation may reform or destroy the soliton state. In the normal dispersion regime, the dissipative solitons, which are the counterpart of Kerr solitons, demonstrated a variety of collision phenomena, including elastic unaltered crossing [59,74–76], as well as inelastic soliton fusion, annihilation, and explosion [77–79]. Collision annihilation and quenching can also occur for cavity solitons and microcavity soliton series, depending heavily on their driving fields [80,81]. On the contrary, Kerr solitons from mode-locked cavities during collision are milder and less variable. Among the predictions of soliton collisions in Manakov systems [27,32,35,37], the energy transfer between solitons and frequency shifts was definitely verified in 2007 [82]. Only recently was the annihilation or fusion of one colliding soliton reported [67–69,71], seemingly in agreement with predictions [32,35]. The inelastic collisions mentioned above commonly occur in the regime of less stable lasing with significant energy transfer. The robustness or the regular soliton behaviors may be an outcome of the conservation of multiple charges (infinite in ideal cases) derived from integrable NSEs, such as energy and momentum [33,83]. Conservations still hold approximately even in dissipative cases of the GLE [14]. The conservations actually provide another lasing pattern with cycling of solitons but require a balance between soliton annihilation or quenching and regeneration in a stable dissipative regime. In this scenario, the motional solitons are greatly weakened, making them fragile to disturbances, which allows for the observation and exploration of massive soliton inelastic collisions. For effective experimental observation, pulse collisions should be controllable and persistent in a cavity configuration, enabling dual- and even multiple-color soliton excitation, which might be stable [15,69,84], unstable (asynchronous pulse trains) [79], or metastable (some weakly mode-locked states) [68]. However, the drawback of these choices is that they either yield limited colliding outcomes or provide inadequate colliding samples. Hence, an appropriate two-color soliton platform facilitates uncovering large-scale inelastic correlations and the origins of two types of collision-induced extreme evolutions: energy depleting (annihilation or collapse) and heightening (fission, explosion [78,79,85,86]),

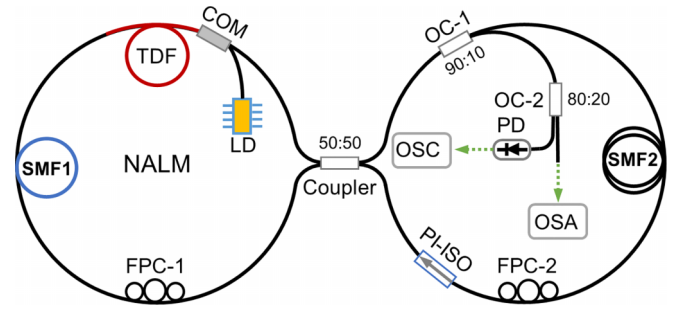


FIG. 1. Schematic of the experimental setup of a figure-8 TDF Laser.

where only the former is considered in this paper. In this study, we utilize a figure-8 Tm-doped fiber (TDF) laser as a test bed to create a featured two-color (bidirectional) soliton source based on our previous work [87]. This soliton source can outpour solitons with a fixed frequency difference to initiate the diverse collision events under consideration. We first generate the bidirectional soliton rains (SRs) in the TDF laser mode locked by the nonlinear amplification loop mirror (NALM) technique. Second, we demonstrate a collective annihilation of drifting solitons that follows a specific statistical pattern. Furthermore, it shows that the collision-annihilation state can self-sustain for a certain collision lifetime.

## II. EXPERIMENTAL RESULTS

### A. Bidirectional soliton rains

Figure 1 is a sketch of the figure-8 setup of a TDF laser mode locked by the NALM in our experiment. It contains a NALM cavity (left ring) and a unidirectional right ring connected by a  $2 \times 2$  coupler (50:50). One end of a 3.5-m-long TDF is spliced with the combiner (COM), connected to a laser diode (LD) source. A 25-m-long 2- $\mu\text{m}$ -band single-mode fiber (SMF1950, SMF1) and another 100-m-long ordinary single-mode fiber (SMF-28, SMF2) are added to the left and right rings, respectively, to increase and allocate the nonlinear phase shift and dispersion, which renders a net dispersion of about  $10.1 \text{ ps}^2$  for a total cavity length of 133 m. The 10% extraction from a  $2 \times 1$  output coupler (OC-1) is used for the following monitoring. Two fiber polarization controllers (FPC-1, FPC-2) and a polarization-independent isolator (PI-ISO) are inserted into the light path to adjust the pulse polarization and cavity loss. This makes the mode-locking condition rely on both the left ring (NALM) and the right one. Following OC-1, another  $2 \times 1$  coupler (OC-2) with a splitting ratio of 20:80 is inserted, and its 20% output port is coupled to an oscilloscope (DSOS104A, Keysight) or a radio-frequency (rf) analyzer (R&S@FSW, Rode-Schwarz) transformed by a high-speed InGaAs photodetector (ET-5000, ETO). The remaining 80% of the output from OC-2 is for power, spectrum, and autocorrelation acquisition, done, respectively, through an optical power meter (LP-3A, Phycience Opto-electronics Co., Ltd.), a wavelength meter (771A, Bristol), and an autocorrelator (Pulse Check SM1600, APE).

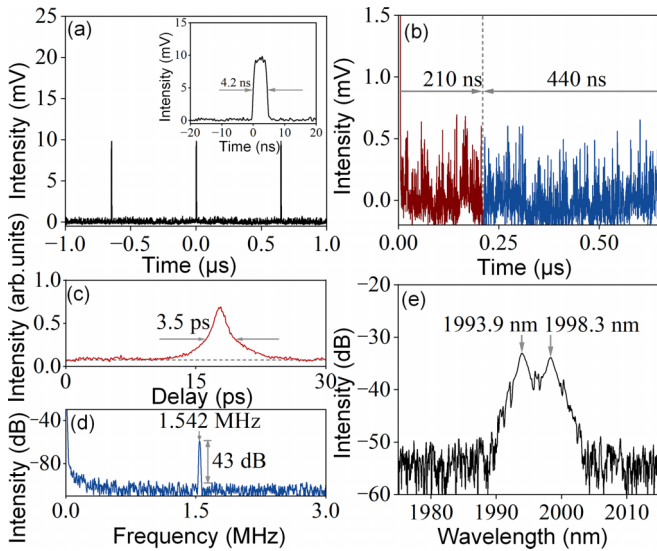


FIG. 2. Bidirectional SR with (a) the pulse train and its condensed phase in the inset, (b) a close-up of f and b solitons in different colors, (c) the autocorrelation trace, (d) the rf signal, and (e) the spectrum.

From the TDF laser schematized in Fig. 1, we obtain a bidirectional full SR in a weak mode-locking state, as shown in Fig. 2. The pulse train in Fig. 2(a) is a typical dual-wavelength soliton series with a pump power of 4.9 W, generated from an initial mode-locking state at a threshold pump power of 3 W. The isolated solitons in the “vapor” component of the SR emerge from both sides of a 4.2-ns-long condensed phase (inset) with different group velocities, forming a two-color soliton source. Figure 2(b) shows the enlarged details of the backward- and forward-drifting solitons, abbreviated as f solitons and b solitons. They occupy the entire cavity and eventually collide at 210 ns relative to the trailing edge, denoted by a dashed line in Fig. 2(b). The fundamental temporal resolution and rf signal analysis are presented in Figs. 2(c) and 2(d), respectively. Since the drifting solitons in the SR are well fed by a high gain to take up the cavity, the drifting solitons surpasses the condensed phase by its weight in the detection of the autocorrelation and spectrum. Therefore, an estimated pulse width of 3.5 ps characterizes primarily the drifting solitons and, to a lesser extent, those in the condensed phase, although they essentially have the same width. These fluctuating solitons, on the other hand, act as “noise” signals, reducing the intensities of rf peaks and thus the signal-to-noise ratio. The fluctuation then accounts for the low rf intensity of 43 dB. The two-color feature of the SR can also be confirmed by the spectrum in Fig. 2(e), where two typical soliton peaks appear atop a spectral pedestal [87]. The higher soliton peak with a shorter wavelength corresponds to the f solitons occupying most of the time window (440 ns), while the lower soliton peak is from the short b-soliton train with a longer wavelength.

### B. Soliton collisions

The two-color SR provides an opportunity to observe postcollision behaviors. It is intriguing to see how two soliton

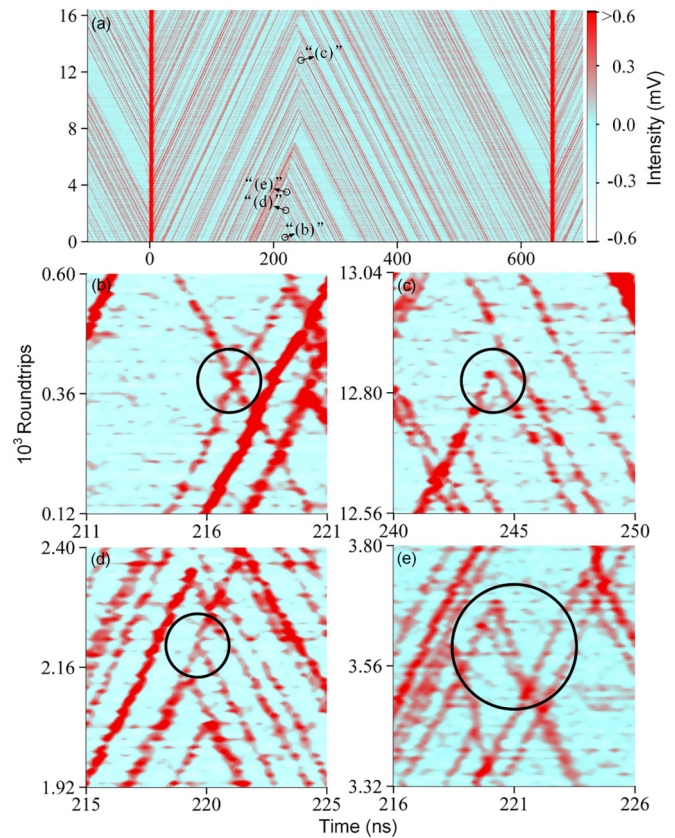


FIG. 3. (a) Collision diagram of one period and four branch scenarios: (b) elastic, (c) collision annihilation, (d) one-sided collision annihilation (fusion), and (e) collision dissociation, zoomed in on (a).

groups develop when they collide head-on. The following experiment shows that annihilation cases dominate in the aftermath of collisions, which clearly deviates from expectations. Under the same polarization control and pumping conditions as before, a trace evolution of the SR presents various collision cases in Fig. 3. Figure 3(a) shows the pulse traces over one period across 16 384 round trips, which are recorded only every 8 round trips due to a limitation of the sampling rate. It was found that each drifting soliton group is quasisteady as a soliton supermolecule, with “atoms” being bound together. The two quasisteady states persist until they intersect, illustrating the collective annihilation of the solitons through multiple collisions. Despite the similar speeds and densities of the two types of solitons, the position of the collision wiggles with time due to the nonuniform distribution of solitons and their varying lifetimes. The observed collision events that occur in Fig. 3(a) can be classified into four cases, which are listed in Figs. 3(b) to 3(e). The case in Fig. 3(b) is a typical elastic collision with an unaltered crossing that can easily be generated in anomalous dispersion fibers. The complete collision annihilation is depicted in Fig. 3(c), representing a highly dissipative scenario in which both solitons annihilate simultaneously, which has never been observed in the mode-locking cavity. The case in Fig. 3(d) is a one-sided collision annihilation or fusion, in which only one soliton is destroyed after it collides with another soliton or soliton molecule. Figure 3(a) also contains a special

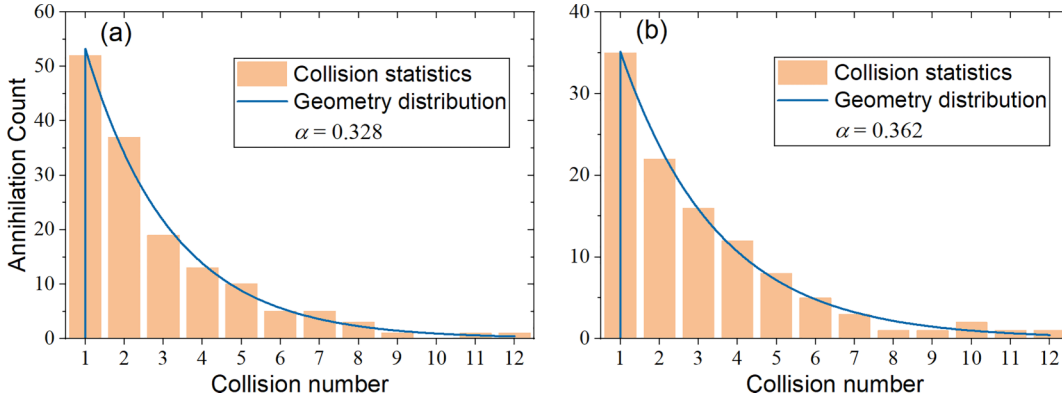


FIG. 4. Collision-annihilation statistics for (a) b solitons and (b) f solitons, fitted with corresponding geometry distributions.

collision between a single soliton and a soliton molecule which was already elaborated on in Refs. [67–69,71]. The collision in Fig. 3(e) belongs to an inelastic collision (collision dissociation) without annihilation, a dissociation of a soliton molecule. In this scenario, the singlet maintains its velocity and just expels the trailing soliton in the molecule into another traveling mode, which differs from the common bond exchange and dissociation described in Refs. [69–71]. Over the known elastic collisions, no steady energy transfer (discernible change in intensity) between solitons is found. The drifting solitons may potentially undergo elastic interactions from previous collision processes but, ultimately, cannot escape the fate of disintegration. This collision-annihilation ending emerges as a different path of the energy balance in the cycling of SRs.

From Fig. 3, we can see that all the drifting solitons collectively annihilate at the front line (collision zone). However, the number of collisions of an individual soliton is unpredictable, ranging from 1 to more than 10. There is an apparent randomness that may arise from variations in coherence and polarization, which supports a statistical analysis. Assuming the independence of collisions, the concept of soliton lifetime will give rise to a specific statistical distribution, which can be supported by collision experiments. In the following derivation, only a few concise results are presented, with detailed information provided in the Appendix. Taking  $\alpha$  as the probability of soliton annihilation for each collision and  $n - 1$  as the number of collisions a soliton undergoes before annihilation in the  $n$ th collision, the survival probability of the soliton follows a geometric distribution,

$$P(n) = \alpha(1 - \alpha)^{n-1}. \quad (1)$$

Therefore, the collision lifetime is an expectation of  $n$ ,

$$\bar{n} = \sum_n nP(n) = 1/\alpha. \quad (2)$$

To verify the distribution above, we present the statistics of soliton annihilation in Fig. 4, resolved from the traces in Fig. 3. The collision events involving soliton molecules are estimated based on intensity variations while indistinguishable fuzzy traces are excluded. The data conform solidly to the geometry distributions, and the statistics suggest that colliding solitons have an annihilation probability of nearly one third (Fig. 4), equivalent to a collision lifetime of about

3. Figure 4 also indicates that there are differences in the lifetimes or annihilation probabilities of the two drifting sides. In addition, both sides consume solitons differently due to dissimilar soliton densities and lifetimes. A stable collision front line requires that

$$\rho_f \Delta v_f \bar{n}_f + \rho_b \Delta v_b \bar{n}_b = 0, \quad (3)$$

where the subscripts f and b indicate the f and b solitons, respectively. In Eq. (3),  $\rho$  represents the soliton density, and  $\Delta v$  is the soliton group velocity relative to the condensed phase  $v$ . The details for deriving Eqs. (2) and (3) can be found in the Appendix. If condition (3) is not satisfied, the collision front line will return to the condensed phase, which changes into a unidirectional (single-color) SR.

The equilibrium condition of Eq. (3) is hard to meet if the cavity is incapable of high stability. A support range in the bidirectional SR regime possibly exists, which can be verified in the experiment. To this end, we slightly vary the pump power from 4.8 to 5.0 W to break the energy equilibrium. A minuscule increase in the pump power leads to a notable change in the SR composition due to the sensitivity of the rain state subject to the cavity energy. The variation is not only the shift of the front line but also an important redistribution of energy: the shrinking of the condensed phase from 7.2 to 4.2 and 3.5 ns with the increase of pump power from 4.8 to 4.9 and 5.0 W, as seen in Fig. 5(a). It can be understood as continued energy transfer of the condensed phase at the trailing edge to the b solitons with the enhancement of pump power, which pushes the front line backward from 75 to 330 ns accordingly. This is illustrated in Figs. 5(b)–5(d), where the rectangular regions indicate the front zones. The energy transfer replenishes the b solitons that are insufficient in number and makes both densities of the bidirectional drifting solitons larger. It should be noted that the relative velocity  $\Delta v_b$  of the b solitons decreases from  $-2.75$  to  $-3.42$  and, finally, to  $-3.61$  km/s and that ( $\Delta v_f$ ) of the f solitons goes down along 4.45, 3.63, and 3.51 km/s with the rise of pump power, where the computation of the group velocities depends on Eq. (A5). The traces in Fig. 3(a) show that the front line is fairly affected by the variation of the soliton number and lifetimes. Through an analysis of the collision dynamics, it is found that the fluctuation width of the front line is proportional to the lifetimes and inversely proportional to the densities of drifting solitons, as described in Eq. (A3). As the soliton densities are increased

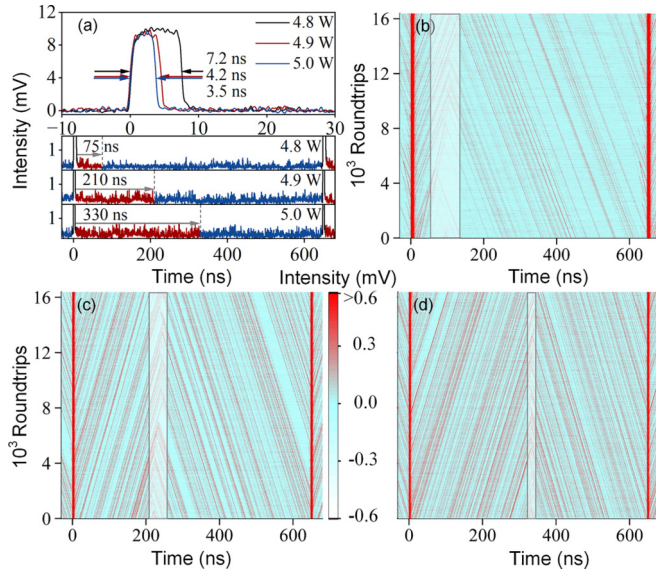


FIG. 5. (a) SR trains with width-reduced condensed phases and shifted front lines under three pump powers and related collision diagrams with pump powers of (b) 4.8, (c) 4.9, and (d) 5.0 W.

on both sides, the width of the front line shrinks accordingly. It should be noted that the reduced fluctuation of the soliton densities also contributes to the narrowing of the front line. These variations governed by Eq. (3) imply that the equilibrium of the collision-annihilation state can be automatically attained. It is not known why the collisions can be preserved by internal self-adaption in such an extreme dissipative case. However, further enhancement of the pump power stops the two-color lasing.

The two-color SR is also observed in a shorter cavity (51 m) and a longer cavity (251 m) by removing and adding to the fibers of SMF-28. The above results can almost be reproduced in a large range of cavity lengths with some changes in the density and group velocity of the drifting solitons. This means that this special SR state can exist in a wide range of anomalous dispersion and cavity loss. While the collision lifetimes have almost constant values in our experiment, it is conceivable to have a different statistical distribution that would lead to varying lifetimes in another laser system. A parametrization of the probability distribution may imply a fundamental law governing the interaction of vector solitons. The mechanism and induced statistics of collective collision annihilation are worth focusing on, which may lead to a collision-selective technique for soliton manipulation.

### C. Polarization difference

Restrained by the polarized cavity elements, the wavelength difference results in polarization divergence between the two soliton groups. According to early collision simulations for passive fibers [27,32,88], polarization is a critical factor in causing energy variation of solitons. With a pump of 5.0 W, it is preliminarily tested here using a polarization beam splitter (PBS), inserted after OC-2, as shown in Fig. 6. When tuning the PBS towards an optimal direction, it is found that in the channel of the horizontal polariza-

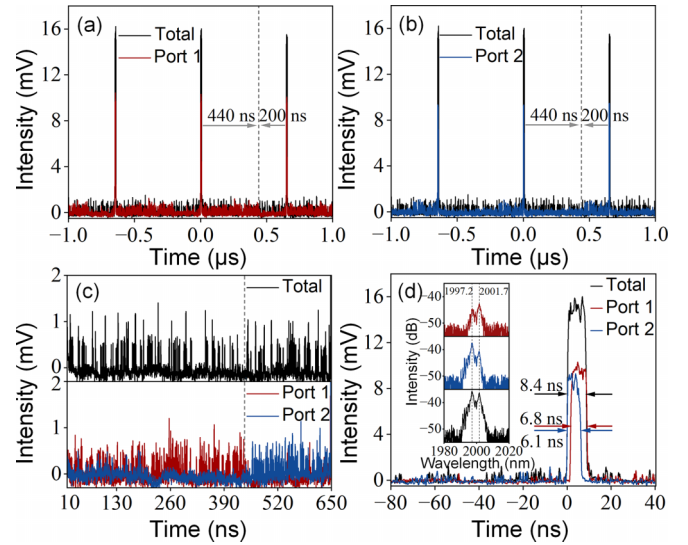


FIG. 6. SR trains through (a) the horizontal and (b) the vertical OCs of the PBS with (c) a close-up of the drifting f and b solitons divided by a front (dashed) line and (d) the condensed phases with corresponding spectra.

tion (port 1), the b solitons reach maximum output while the f solitons are substantially suppressed. Conversely, in the vertical channel (port 2), the opposite occurs. This can be seen in Figs. 6(a) and 6(b), where the front line shifts backward compared to Fig. 5. Figure 6(c) provides the details of the drifting solitons captured from Figs. 6(a) and 6(b). In Fig. 6(c), the light extinction is accompanied by wavelength suppression, indicated by the two-color spectral peaks shown in the inset of Fig. 6(d). The background SR train, drawn as black curves, is a polarization-unresolved pulse used as a reference signal. Figure 6(d) indicates the polarization composition of the condensed phase. As expected, the f solitons gather at the front of the pulse, while the b solitons reside at the back, where the time calibration of the two polarized condensed phases is determined by the timing of soliton release. It can also be seen from the two channels that the intensities and pulse widths of the main pulses are reduced as well. The reduction in the durations of the two polarized components suggests a transition of polarization from the leading edge to the trailing part within the condensed phase. The two soliton groups are found to be heterogeneous because they have different elliptical polarizations, with their principal axes being nearly orthogonal. However, both soliton groups can deviate from their original polarizations over time since the suppression by the PBS can gradually change.

The annihilation, which is also associated with lumped cavity modulation, cannot be fully elucidated by the polarization mechanism [67,88,89] or a simple energy transfer [27,32,44,57,66,82] within the framework of coupled NSEs and GLEs. An effective explanation of the experiments here has to depend on a nonintegrable non-Hamilton model, involving necessary dissipative factors and polarization dynamics.

It is expected that the results in this paper will shed light on the nonequilibrium statistical mechanics of other

soliton ensembles, such as those in Bose-Einstein condensation, hydrodynamics, and chemical reactions, when they can be governed by (“1 + 1”)-dimensional coupled NSEs. Practically, the collective annihilation mechanism should be further developed based on its potential impact on soliton-based optical data processing. On the one hand, it can be utilized to promote soliton-manipulating technology. On the other hand, we quote Grellu’s concluding remarks from Ref. [90]: “Exploring bifurcations and non-stationary dynamics, beyond being fun fundamental science, also represents a way to develop better control strategies.” Hence, understanding how to effectively bypass the SR states or convert them into regular bound soliton patterns or two-color frequency combs is practically relevant.

### III. CONCLUSIONS

In summary, an intriguing collective collision annihilation was triggered in a two-color vector SR state inside a figure-8 TDF laser, weakly mode locked under high-gain conditions. Four soliton collision scenarios emerged from the collision traces. The statistical analysis demonstrated that two-color solitons exhibit average annihilation lifetimes between 3 and 4 and maintain self-sustaining collisions without degeneration. The findings in this paper will enhance our understanding of the complexity of solitons in collective dissipative dynamics and are expected to draw attention to the underlying mechanism.

### ACKNOWLEDGMENTS

This work was supported by the National Natural Science Foundation of China (Grants No. 62275194 and No. 61775166), the Natural Science Foundation of Tianjin (Grant No. 19JCZDJC32600), and the Program for Innovative Research Team at the universities of Tianjin (Grant No. TD13-5035).

### APPENDIX: COLLISIONAL STATISTICS

The geometric distribution has a discrete random variable  $X$  of integers [91], i.e.,

$$P(X = n) = \alpha(1 - \alpha)^{n-1}, \quad X \in \mathbb{Z}^+, \quad (\text{A1})$$

where  $\alpha$  is the probability of success (annihilation) through independent Bernoulli trials (collisions). In Eq. (A1), it is assumed that no soliton will be affected by a past collision due to its robustness, which makes the colliding solitons memoryless. In fact, phase variations across an elastic collision are inevitable, which, nevertheless, has negligible relevance in the collisional statistics here. The expected value of  $X$  is

$$\begin{aligned} E(X) = \bar{n} &= \sum_{n=1}^{\infty} nP(n) = \sum_{n=1}^{\infty} n\alpha(1 - \alpha)^{n-1} \\ &= -\alpha \frac{d}{d\alpha} \sum_{n=1}^{\infty} (1 - \alpha)^n = \alpha^{-1}. \end{aligned} \quad (\text{A2})$$

This means a soliton will be annihilated after an average number of collisions  $\bar{n} = 1/\alpha$ , the average collision lifetime. By a similar trick, the variance of  $X$  can be found to be  $(1 - \alpha)/\alpha^2$ .

When the collision annihilation remains as an equilibrium state, the same number of solitons as in the production from the condensed phase will be exhausted at the same time. It then stabilizes the front line in the middle of the SR. The number of solitons entering the front line within a time interval  $\Delta t$  is proportional to the soliton density  $\rho$  (the soliton number in a unit length of fiber) and to the relative group velocity of solitons  $\Delta v$  in reference to the condensed phase. A stable front line requires that the number of collisions from both sides should be the same, i.e.,  $\rho|\Delta v|\bar{n}\Delta t$ , where the lifetime  $\bar{n}$  also represents the effective number of collisions provided by every soliton. This straightforwardly leads to condition (3), which serves as the premise for subsequent development.

Referring to the general molecular collision model [92], the size of the front line is predictable according to the known probability distribution. The average collisional time interval of one  $f$  soliton with two consecutive  $b$  solitons differs from that of one  $b$  soliton with two following  $f$  solitons, but it can be uniformly written as  $1/(\rho_{b/f}\Delta v_R)$ , where  $\Delta v_R = |\Delta v_f - \Delta v_b|$  is the relative speed of the two types of solitons. Here, the probability of soliton annihilation is so high that the densities of bidirectional solitons can be approximated as constants. The transit time of one  $f$  or  $b$  soliton across the front zone is then

$$\tau_{f/b} = \frac{\bar{n}_{f/b}}{\rho_{b/f}\Delta v_R}. \quad (\text{A3})$$

The forward and backward mean free paths have the same magnitude, which can be derived from Eq. (A3) by a direct product,

$$l_p = \tau_{f/b}|\Delta v_{f/b}| = \frac{\rho_{f/b}\bar{n}_{f/b}|\Delta v_{f/b}|}{\rho_f\rho_b\Delta v_R}, \quad (\text{A4})$$

where it can be seen that the last expression remains unchanged when switching between the  $f$  and  $b$  cases, considering Eq. (3). The width of the front line can be estimated as the mean free path  $l_p$  or as an average of the transit times  $(\tau_f + \tau_b)/2$ . If the soliton densities are unevenly distributed, the front line will curve accordingly.

In the above results, the relative velocities  $\Delta v_{f/b/R}$  are a lot smaller than that of the condensed phase  $v$  and can be estimated from the collision diagrams. Setting the slope of the soliton traces in one direction as  $S$ , the number of round trips per second, we can find the number of round trips over the time when a soliton travels from one side of the condensed phase to the other side and back to the starting point, i.e.,  $R = TS$ , with  $T$  being the cavity round-trip time. This means that when a soliton travels one round trip forward or backward relative to the condensed phase, the condensed phase will circle the cavity by the number of  $R$ , as implied by the speed ratio  $v : \Delta v_{f/b}$ . So we have

$$\Delta v_{f/b} = vR_{f/b}^{-1}. \quad (\text{A5})$$

In our work, the collision lifetime is quite small. It is possible that the lifetime is greatly enhanced when elastic collisions dominate. In this case, the discrete distribution will naturally be replaced by a continuous one. This can be accomplished by establishing an asymptotic correspondence between the number of collisions and a spatial dimension. Converting discreteness to continuity can be thought of as reducing an

effective lifetime  $\alpha/m$  in a limiting process of increasing the number  $m$ . Then, the probability mass function  $P(n)$  becomes

$$P_m(n) = \frac{\alpha}{m} \left(1 - \frac{\alpha}{m}\right)^{\frac{\alpha}{m}m-1}, \quad (\text{A6})$$

where the number  $m$  can be regarded as the maximum number of collisions that a soliton possibly has in the front zone. For the degenerate case of one-sided collision annihilation, in which the lifetime of  $b$  solitons approaches zero, the distribution can be simplified. By introducing a distance variable  $z$ ,  $n/m = \eta z$  with a constant coefficient  $\eta$ , Eq. (A6) tends to a density function of the exponential distribution,

$$\begin{aligned} P_m(n) &= \alpha \eta dz \left(1 - \frac{\alpha}{m}\right)^{\frac{\alpha}{m} \alpha \eta z - 1} \xrightarrow{m \rightarrow \infty} \beta \exp(-\beta z) dz \\ &\equiv f(z) dz, \quad \beta = \alpha \eta. \end{aligned} \quad (\text{A7})$$

The survival probability of the  $f$ -soliton flux at position  $z$  is

$$F(z) \equiv 1 - \int_0^z f(\zeta) d\zeta = \exp(-\beta z), \quad (\text{A8})$$

where  $\beta$  represents the ‘‘absorption coefficient’’ of the  $f$  solitons and the variable  $z$  ranges from the trailing edge,  $z = 0$ , to the leading edge,  $z = z_0$ , of the condensed phase in the relative frame. The exponential distribution is then in accord with the common absorption law (Lambert-Beer law) and gas collision statistics, such as those in collisional excitation, ionization, and combination reaction. In a general bidirectional collision-annihilation case, the soliton densities are position dependent due to annihilation, i.e.,  $\rho_{f/b}(z) = \rho_{0f/b} \hat{\rho}_{f/b}(z)$ , where the constants  $\rho_{0f/b}$  are the initial densities. Therefore, the number of

collisions  $n$  corresponds to two integrations

$$n_f \rightarrow \rho_{0b} \int_0^z \hat{\rho}_b(\zeta) d\zeta, \quad n_b \rightarrow \rho_{0f} \int_z^{z_0} \hat{\rho}_f(\zeta) d\zeta. \quad (\text{A9})$$

$\rho_{0f/b}$  are sufficiently large to be comparable to  $m$ , allowing them to be simply expressed as  $\eta_{f/b} m$ . In this way, Eq. (3) can be reformulated as  $\Delta v_f / \beta_f = \Delta v_b / \beta_b$ , where the densities of solitons in Eq. (3) should be the initial densities  $\rho_{0f/b}$ . From Eq. (A6), the probabilities of annihilation for bidirectional soliton fluxes evolve into

$$\begin{aligned} f_f(z) &= N_f \beta_f \exp \left[ -\beta_f \int_0^z \hat{\rho}_b(\zeta) d\zeta \right] \hat{\rho}_b(z), \\ f_b(z) &= N_b \beta_b \exp \left[ -\beta_b \int_z^{z_0} \hat{\rho}_f(\zeta) d\zeta \right] \hat{\rho}_f(z), \end{aligned} \quad (\text{A10})$$

where  $N_{f/b}$  are the coefficients of distribution normalization and  $\beta_{f/b} = \alpha_{f/b} \eta_{b/f}$ . Obviously, the function  $f_f(z)$  transforms into Eq. (A7) in the case of one-sided forward collision annihilation with  $\hat{\rho}_b(\zeta) \rightarrow 1$ . It can easily be found that the stable soliton densities satisfy

$$\hat{\rho}'_f = -\hat{\rho}_f f_f, \quad \hat{\rho}'_b = \hat{\rho}_b f_b, \quad (\text{A11})$$

where the prime symbol represents the derivative with respect to  $z$ . Due to the complexity of the integro-differential equation, only the numerical solution of Eq. (A11) is attainable. The width of the collisional zone is difficult to calculate in this case but can be roughly estimated as

$$l_p \sim \beta_{f/b}^{-1} \quad (\text{A12})$$

based on the exponential distribution.

- 
- [1] T. Dauxois and M. Peyrard, *Physics of Solitons* (Cambridge University Press, Cambridge, 2015).
- [2] Y. Song, X. Shi, C. Wu, D. Tang, and H. Zhang, *Appl. Phys. Rev.* **6**, 021313 (2019).
- [3] G. P. Agrawal, *Nonlinear Fiber Optics* (Academic, New York, 2001); *Applications of Nonlinear Fiber Optics* (Academic, New York, 2008).
- [4] F. Amrani, M. Salhi, H. Leblond, and F. Sanchez, *Opt. Commun.* **283**, 5224 (2010).
- [5] F. Amrani, A. Haboucha, M. Salhi, H. Leblond, A. Komarov, and F. Sanchez, *Appl. Phys. B* **99**, 107 (2010).
- [6] F. Amrani, M. Salhi, P. Grelu, H. Leblond, and F. Sanchez, *Opt. Lett.* **36**, 1545 (2011).
- [7] D. A. Korobko, R. Gumenyuk, I. O. Zolotovskii, and O. G. Okhotnikov, *Opt. Fiber Technol.* **20**, 593 (2014).
- [8] A. Komarov, F. Amrani, A. Dmitriev, K. Komarov, D. Meshcheriakov, and F. Sanchez, *Phys. Rev. A* **85**, 013802 (2012).
- [9] J. P. Gordon, *J. Opt. Soc. Am. B* **9**, 91 (1992).
- [10] E. A. Kuznetsov, A. V. Mikhailov, and I. A. Shimokhin, *Physica D: Nonlinear Phenomena* **87**, 201 (1995).
- [11] H. A. Haus, F. I. Khatri, W. S. Wong, E. P. Ippen, and K. R. Tamura, *IEEE J. Quantum Electron.* **32**, 917 (1996).
- [12] R. Weill, A. Bekker, V. Smulakovsky, B. Fischer, and O. Gat, *Phys. Rev. A* **83**, 043831 (2011).
- [13] Q.-H. Park and H. J. Shin, *Phys. Rev. Lett.* **82**, 4432 (1999).
- [14] J. J. Huang, Z. L. Jia, and X. L. Zhang, *Phys. Rev. A* **105**, 053526 (2022).
- [15] Y. Wei, B. Li, X. Wei, Y. Yu, and K. K. Y. Wong, *Appl. Phys. Lett.* **112**, 081104 (2018).
- [16] S. Chouli and P. Grelu, *Phys. Rev. A* **81**, 063829 (2010).
- [17] V. M. Krasnov, *Phys. Rev. B* **85**, 134525 (2012).
- [18] J. H. V. Nguyen, P. Dyke, D. Luo, Boris A. Malomed, and R. G. Hulet, *Nat. Phys.* **10**, 918 (2014).
- [19] S. Lannig, C.-M. Schmied, M. Prüfer, P. Kunkel, R. Strohmaier, H. Strobel, T. Gasenzer, P. G. Kevrekidis, and M. K. Oberthaler, *Phys. Rev. Lett.* **125**, 170401 (2020).
- [20] D. W. Aossey, S. R. Skinner, J. L. Cooney, J. E. Williams, M. T. Gavin, D. R. Andersen, and K. E. Lonngren, *Phys. Rev. A* **45**, 2606 (1992).
- [21] F. Xin, F. Di Mei, L. Falsi, D. Pierangeli, C. Conti, A. J. Agranat, and E. DelRe, *Phys. Rev. Lett.* **127**, 133901 (2021).
- [22] X. Hu, J. Ma, L. M. Zhao, J. Guo, and D. Y. Tang, *Opt. Express* **29**, 12590 (2021).
- [23] J. Scheuer and M. Orenstein, *J. Opt. Soc. Am. B* **18**, 954 (2001).
- [24] J. P. Gordon, *Opt. Lett.* **8**, 596 (1983).
- [25] F. M. Mitschke and L. F. Mollenauer, *Opt. Lett.* **12**, 355 (1987).
- [26] P. A. Andrekson, N. A. Olsson, P. C. Becker, J. R. Simpson, T. Tanbun-Ek, R. A. Logan, and K. W. Wecht, *Appl. Phys. Lett.* **57**, 1715 (1990).
- [27] C.-J. Chen, P. K. A. Wai, and C. R. Menyuk, *Opt. Lett.* **15**, 477 (1990).
- [28] M. Eguchi, K. Hayata, and M. Koshiba, *Opt. Lett.* **16**, 82 (1991).
- [29] Y. S. Kivshar and B. A. Malomed, *Rev. Mod. Phys.* **61**, 763 (1989).
- [30] B. A. Malomed, *J. Opt. Soc. Am. B* **9**, 2075 (1992).

- [31] Q. Wang, P. K. A. Wai, C.-J. Chen, and C. R. Menyuk, *Opt. Lett.* **17**, 1265 (1992).
- [32] B. A. Malomed and S. Wabnitz, *Opt. Lett.* **16**, 1388 (1991).
- [33] X. D. Cao and C. J. McKinstrie, *J. Opt. Soc. Am. B* **10**, 1202 (1993).
- [34] X. D. Cao and D. D. Meyerhofer, *J. Opt. Soc. Am. B* **11**, 380 (1994).
- [35] R. Radhakrishnan, M. Lakshmanan, and J. Hietarinta, *Phys. Rev. E* **56**, 2213 (1997).
- [36] C. De Angelis and S. Wabnitz, *Opt. Commun.* **125**, 186 (1996).
- [37] R. Radhakrishnan, P. T. Dinda, and G. Millot, *Phys. Rev. E* **69**, 046607 (2004).
- [38] J. K. Yang and Y. Tan, *Phys. Rev. Lett.* **85**, 3624 (2000).
- [39] R. Radhakrishnan and M. Lakshmanan, *J. Phys. A* **28**, 2683 (1995).
- [40] W.-J. Liu, B. Tian, H.-Q. Zhang, L.-L. Li, and Y.-S. Xue, *Phys. Rev. E* **77**, 066605 (2008).
- [41] X. Liu, H. Triki, Q. Zhou, W. Liu, and A. Biswas, *Nonlinear Dyn.* **94**, 703 (2018).
- [42] X.-W. Yan and Y. Chen, *Appl. Math. Lett.* **125**, 107737 (2022).
- [43] Q. Zhou, Z. Huang, Y. Sun, H. Triki, W. Liu, and A. Biswas, *Nonlinear Dyn.* **111**, 5757 (2023).
- [44] M. Wang, W.-R. Shan, X. Lü, Y.-S. Xue, Z.-Q. Lin, and B. Tian, *Appl. Math. Comput.* **219**, 11258 (2013).
- [45] T. Kanna and M. Lakshmanan, *Phys. Rev. Lett.* **86**, 5043 (2001).
- [46] T. Kanna and M. Lakshmanan, *Phys. Rev. E* **67**, 046617 (2003).
- [47] T. Kanna, M. Lakshmanan, P. T. Dinda, and N. Akhmediev, *Phys. Rev. E* **73**, 026604 (2006).
- [48] Y. Jiang, B. Tian, W.-J. Liu, K. Sun, M. Li, and P. Wang, *Phys. Rev. E* **85**, 036605 (2012).
- [49] T. Kanna and M. Lakshmanan, *Eur. Phys. J. B* **29**, 249 (2002).
- [50] P. T. Dinda, R. Radhakrishnan, and T. Kanna, *J. Opt. Soc. Am. B* **24**, 592 (2007).
- [51] M. Vijayajayanthi, T. Kanna, and M. Lakshmanan, *Phys. Rev. E* **108**, 054213 (2023).
- [52] I. E. Papacharalampos, P. G. Kevrekidis, B. A. Malomed, and D. J. Frantzeskakis, *Phys. Rev. E* **68**, 046604 (2003).
- [53] C. I. Christov, S. Dost, and G. A. Maugin, *Phys. Scr.* **50**, 449 (1994).
- [54] M. D. Todorov and C. I. Christov, *Conf. Public.* **2007**, 982 (2007).
- [55] Q.-B. Xu and Q.-S. Chang, *Acta Math. Appl. Sin., Engl. Ser.* **26**, 205 (2010).
- [56] P. Zhang, W. Hu, Z. Wang, and Z. Qiao, *J. Nonlinear Math. Phys.* **30**, 1467 (2023).
- [57] P. Balla and G. P. Agrawal, *Phys. Rev. A* **98**, 023822 (2018).
- [58] M. D. Todorov and C. I. Christov, *Math. Comput. Simul.* **80**, 46 (2009).
- [59] N. Akhmediev, J. M. Soto-Crespo, M. Grapinet, and P. Grelu, *Opt. Fiber Technol.* **11**, 209 (2005).
- [60] M. D. Todorov, *Math. Comput. Simul.* **127**, 273 (2016).
- [61] K. Goda and B. Jalali, *Nat. Photonics* **7**, 102 (2013).
- [62] A. Mahjoubfar, D. V. Churkin, S. Barland, N. Broderick, S. K. Turitsyn, and B. Jalali, *Nat. Photonics* **11**, 341 (2017).
- [63] G. Herink, F. Kurtz, B. Jalali, D. R. Solli, and C. Ropers, *Science* **356**, 50 (2017).
- [64] K. Krupa, K. Nithyanandan, U. Andral, P. Tchofo-Dinda, and P. Grelu, *Phys. Rev. Lett.* **118**, 243901 (2017).
- [65] F. Copie, P. Suret, and S. Randoux, *Opt. Commun.* **545**, 129647 (2023).
- [66] K. Zhao, C. Gao, X. Xiao, and C. Yang, *Photonics Res.* **9**, 289 (2021).
- [67] A. Klein, S. Meir, H. Duadi, A. Govindarajan, and M. Fridman, *Opt. Express* **29**, 18512 (2021).
- [68] H. Liang, X. Zhao, B. Liu, J. Yu, Y. Liu, R. He, J. He, H. Li, and Z. Wang, *Nanophotonics* **9**, 1921 (2020).
- [69] J. Li, H. Li, Z. Wang, Z. Zhang, S. Zhang, and Y. Liu, *Photonics* **9**, 489 (2022).
- [70] J. He, P. Wang, R. He, C. Liu, M. Zhou, Y. Liu, Y. Yue, B. Liu, D. Xing, K. Zhu, K. Chang, and Z. Wang, *Opt. Express* **30**, 14218 (2022).
- [71] J. He, M. Zhou, C. Liu, P. Wang, D. Xing, J. Li, Y. Liu, and Z. Wang, *Opt. Express* **31**, 22776 (2023).
- [72] J. Zeng and M. Y. Sander, *Opt. Express* **30**, 7894 (2022).
- [73] R. Liu, D. Zou, S. Niu, Y. Song, and M. Hu, *Opt. Express* **31**, 1452 (2023).
- [74] P. Grelu and N. Akhmediev, *Opt. Express* **12**, 3184 (2004).
- [75] M. Olivier, V. Roy, M. Piché, and F. Babin, *Opt. Lett.* **29**, 1461 (2004).
- [76] V. Roy, M. Olivier, F. Babin, and M. Piché, *Phys. Rev. Lett.* **94**, 203903 (2005).
- [77] Y. Zhou, Y.-X. Ren, J. Shi, H. Mao, and K. K. Y. Wong, *Optica* **7**, 965 (2020).
- [78] J. Peng and H. Zeng, *Commun. Phys.* **2**, 34 (2019).
- [79] Z. Guo, T. Liu, and H. Zeng, *Adv. Photonics Res.* **3**, 2200082 (2022).
- [80] K. Luo, J. K. Jang, S. Coen, S. G. Murdoch, and M. Erkintalo, *Opt. Lett.* **40**, 3735 (2015).
- [81] W. Weng, R. Bouchand, and T. J. Kippenberg, *Phys. Rev. X* **10**, 021017 (2020).
- [82] D. Rand, I. Glesk, C.-S. Brès, D. A. Nolan, X. Chen, J. Koh, J. W. Fleischer, K. Steiglitz, and P. R. Prucnal, *Phys. Rev. Lett.* **98**, 053902 (2007).
- [83] J. Kim, Q.-H. Park, and H. J. Shin, *Phys. Rev. E* **58**, 6746 (1998).
- [84] H. Zhao, Y. Zhu, F. Xiang, X. Sun, L. Jin, S. Y. Set, and S. Yamashita, in *2020 Asia Communications and Photonics Conference (ACP) and International Conference on Information Photonics and Optical Communications (IPOC)*, Beijing, China (IEEE, 2020), p. M4A.72.
- [85] P. Ryczkowski, M. Närhi, C. Billet, J.-M. Merolla, G. Genty, and J. M. Dudley, *Nat. Photonics* **12**, 221 (2018).
- [86] F. Lu, Q. Lin, W. H. Knox, and G. P. Agrawal, *Phys. Rev. Lett.* **93**, 183901 (2004).
- [87] J. Huang, X. Liu, J. Lin, and X. Zhang, *Opt. Laser Technol.* **169**, 110092 (2024).
- [88] M. D. Todorov and C. I. Christov, *Math. Comput. Simul.* **82**, 1321 (2012).
- [89] H. Lan, F. Chen, Y. Wang, M. Klimczak, R. Buczynski, X. Tang, M. Tang, H. Zhu, and L. Zhao, *Opt. Express* **31**, 21452 (2023).
- [90] P. Grelu, *Opt. Commun.* **552**, 130035 (2024).
- [91] M. Lefebvre, *Applied Probability and Statistics* (Springer, New York, 2006).
- [92] R. P. Feynman, R. B. Leighton, and M. Sands, *The Feynman Lectures on Physics* (California Institute of Technology, New York, 2010), Vol. 1.